

1. Specific Aims

1.0 Introduction

This research proposal targets the development of the first portable intra-operative digital specimen tomosynthesis system for rapid and accurate three-dimensional radiographic margin assessment of surgically excised breast tissue specimens during breast-conserving surgery.

Conventional two-dimensional projection specimen radiography is currently one of the most widely used techniques for intra-operative macroscopic margin assessment; however a clinical intra-operative digital specimen tomosynthesis system does not yet exist. Despite its wide spread use, the sensitivity and specificity of projection specimen radiography is relatively low when compared to the gold standard of permanent section histopathology, in the range of 52% and 85%, respectively¹. While specimen radiography will probably never match the sensitivity and specificity of permanent section histopathology due to possibility of microscopic disease at specimen margins which are not detectable by radiography, intra-operative radiographic sensitivity and specificity can be improved by addressing the well-documented impact of tissue overlap associated with projection imaging, which can obscure lesions^{2,3,4,5} generating false-negatives⁶, as well as mimicking of masses by the superimposition of normal tissues, which can generate false-positives⁷.

We hypothesize that specimen tomosynthesis will significantly improve the sensitivity and specificity of intra-operative excision margin assessment in breast-conserving surgery by providing rapid and accurate three-dimensional radiographic margin information to the physician. In addition to lowering re-excision and local recurrence rates associated with breast-conserving surgery through more accurate intra-operative excision margin assessment, ex-vivo specimen tomosynthesis could also potentially present a unique opportunity as a relatively simple clinical test-bed to assess the true clinical efficacy of digital tomosynthesis in imaging of breast tissue, thus aiding the development and optimization of clinical full-breast tomosynthesis systems for screening mammography.

Though much research continues in digital tomosynthesis for screening mammography, a clinical breast screening tomosynthesis system is not yet available. This is partially due to the special complexities associated with breast tomosynthesis, including the trade-off between image quality and patient dose, as well as mechanical challenges associated with the rotation of a heavy x-ray tube assembly around the patient. In specimen tomosynthesis, it would be possible to simply rotate the specimen with respect to a fixed x-ray source and a fixed detector, as opposed to rotating the heavy x-ray gantry around the patient. Furthermore, with an x-ray shielded, portable cabinet x-ray system, it would also be possible to acquire a very high quality tomosynthesis image sequence in a clinically acceptable time period and without concern for patient dose.

While there are several commercially available micro-Computed Tomography (CT) systems^{8,9,10}, none are optimized for intra-operative specimen imaging due to long image acquisition times and very high costs. The use of micro-CT systems for intra-operative margin assessment is therefore extremely rare. Unlike conventional CT and micro-CT, where the source and the detector make a complete 360 degree rotation around the object, in digital tomosynthesis only a small number of discrete exposures are acquired around a smaller rotation angle (typically 10 to 15 exposures acquired within +/- 15 degrees). In applications such as breast-conserving surgery or mammography, where a lower resolution (on the order of 1 mm) may be acceptable in the depth dimension while maintaining high spatial resolution in each reconstructed plane (on the order of 50 microns, or 10 line-pairs per mm), tomosynthesis can provide diagnostically useful reconstructed images in a clinically acceptable time period, on the order of two or three minutes.

This research proposal builds upon a prior Phase I grant previously awarded to this Principal Investigator and to this institution in February 2008, grant number 1R43CA133990-01, entitled "Intra-operative margin assessment tool for breast-conserving surgery." This prior grant was towards the development of a novel specimen container for use in breast-conserving surgery. The container was originally designed to enable two orthogonal radiographs of the excised specimen. Specimen tomosynthesis will be a natural progression of two-view imaging of excised specimens, similar to the anticipated evolution of conventional two-view mammography to three-dimensional full breast tomosynthesis. As will be discussed in detail in this document, the specimen container developed under the previous grant will be one of the key components of the breast specimen tomosynthesis system, by suppressing motion and metal artifacts commonly seen in tomosynthesis. In order to minimize motion and metal artifacts, the container is designed to hold the specimen securely in place during tomosynthesis rotation without applying excessive compression, and to provide built-in three-dimensional orientation indicators which eliminate the need for metal localization clips.

1.1 Key concepts and terminology

Breast-conserving surgery (BCS) is commonly defined as the surgical removal of a breast tumor with a safe margin of normal tissue. When supplemented with radiation therapy to manage potential residual microscopic disease, BCS is generally referred to as breast-conserving therapy, or BCT.

Studies have shown¹¹ no significant difference in survival rates between women treated with radical mastectomy (complete removal of the entire breast, underlying chest muscle, and axillary lymph nodes) and those treated with BCT. However, surgical re-excision rates and local recurrence rates in patients treated with BCT are at least twice as high as those treated with mastectomy^{12,1}.

Since the objective of BCS is not to leave any cancer behind in the breast, obtaining tumor-negative margins when performing BCS is the standard of care to minimize the risk of local recurrence¹³. While disease free excision margins do not guarantee the absence of residual disease, it has been shown that local recurrence is more frequent in patients with positive excision margins than those with negative margins (18.2%, 7.1% and 3.7% in patients with histologically positive, unknown and negative margins, respectively)¹⁴.

Despite the attempt to achieve negative margins, primary excision yields histologically positive margins 20% to 55% of the time¹⁵. Furthermore, permanent section histopathology, the gold standard in determining excision margin status, is generally not available until well after the patient has left the operating room. Thus, patients with histologically positive margins must often return to the hospital for surgical re-excision(s).

A three-dimensional radiographic margin assessment system, which can reliably predict macroscopic excision margin status while the patient is still in the operating room, could therefore help in reducing both surgical re-excision and local recurrence rates associated with BCS.

1.2 Phase I Specific Aims

Specific Aim 1: Specify, design and integrate hardware components of an intra-operative tomosynthesis system optimized for surgically excised breast tissue specimens in BCS.

Key hardware components of a system optimized for specimen tomosynthesis are: a microfocus x-ray source and associated high voltage power supply, a high resolution digital x-ray detector, a precision motorized specimen rotation stage, a lead-shielded portable x-ray cabinet, and an imaging workstation to control and synchronize the operation of each hardware component.

Specific Aim 2: Specify, design and implement reconstruction algorithms optimized for rapid and accurate intra-operative tomosynthesis of surgically excised breast tissue specimens.

Our primary objective is to design and implement tomosynthesis algorithms which will make high resolution, artifact-free, low noise reconstructed tomosynthesis slices of the excised specimen available for review in the operating room and simultaneously in the Radiology and Pathology Departments within two to three minutes of the surgical excision.

Specific Aim 3: Integrate selected hardware and software components optimized for intra-operative tomosynthesis of surgically excised breast tissue specimens.

System integration will yield a seamlessly operating device, where the user will simply place the excised specimen inside the x-ray cabinet, press a single button, and will be presented within two to three minutes with a slice-by-slice display of resultant reconstructed images on a high resolution monitor.

Specific Aim 4: Quantify the integrated system's efficacy in a pre-clinical setting, utilizing simulated excised breast tissue samples and standard breast x-ray imaging phantoms.

Our objective is to design the intra-operative specimen tomosynthesis system to match or exceed the published performance of full-breast tomosynthesis systems in terms of quantitative performance parameters, including signal-to-noise ratio and artifact spread function, as well as image acquisition and reconstruction times.

In Phase I of this research, we will utilize both computer-simulated and physical phantoms to quantify the efficacy of the device and associated software algorithms. In phase II, we will conduct a formal clinical trial to quantify any potential reduction in surgical re-excision rates attributable to the use of the intra-operative specimen tomosynthesis developed and optimized in Phase I.

2. Background and Significance

2.0 Clinical problem statement

Each year, approximately 210,000 women in the United States, and an additional 360,000 women in the European Union are diagnosed with breast cancer^{16, 17}. As a result of long term studies showing no significant difference in the survival rates between women treated with radical mastectomy and those treated with BCT¹⁸, it is estimated that over half the women diagnosed with breast cancer choose the less radical route of BCT over mastectomy to preserve part of their original breast¹⁹. Despite its cosmetic advantages, the risk of local recurrence for patients treated with BCT range from 10% to 40%, as compared to rates of 2% to 8% in mastectomy¹². Furthermore, surgical re-excision rates in BCT, where additional surgery is performed to remove additional tissue from the breast, have been reported to be as high as 20% to 55%¹⁵.

As indicated in the Specific Aims section, while disease free excision margins do not guarantee the absence of residual disease, local recurrence rates of 18.2%, 7.1%, and 3.7% have been correlated with histologically positive, unknown and negative margins respectively¹⁴. Several other studies have shown a strong correlation between excision margin width and residual disease in the breast cavity after excision. Dillon and colleagues have reported²⁰ that residual disease was present in 58%, 56% and 45% of those with tumor-margin distances of <1 mm, 1 mm to 2mm, and 2mm to 5 mm respectively. Holland and colleagues have shown²¹ that of 282 invasive cancers, only 39% had tumors confined to the primary mass. Forty one percent had foci of tumor more than 2 cm beyond the edge of the primary tumor mass. Ten percent had residual foci of invasive or in situ carcinoma even within a 4 cm margin around the primary tumor.

It has been shown that pre-operative Magnetic Resonance Imaging (MRI) can detect intraductal spread of disease more accurately than mammography and ultrasound with a reported sensitivity and specificity for detecting residual disease of 61.2% and 69.7% respectively^{22, 23, 24}. However, several other researchers have questions whether MRI can become a standard component of intra-operative BCS, given the proven efficacy of postoperative radiotherapy in controlling residual disease and the high cost of MRI^{25, 26}.

A simple, low cost, rapid and accurate three dimensional intra-operative radiographic margin assessment system for BCS with the highest possible sensitivity and specificity, such as the specimen tomosynthesis system proposed here, could be a cost-effective means of lowering re-excision and local recurrence rates in BCS.

2.1 State-of-the-art in intra-operative radiographic margin assessment

One of the most commonly utilized technologies for intra-operative macroscopic margin assessment in BCS is specimen radiography. Several companies, including Bioptics, Inc. of Tucson, Arizona, Faxitron X-Ray Corporation of Wheeling, Illinois, and Kubtec Corporation of Fairfield, Connecticut, manufacture portable intra-operative digital projection x-ray imaging systems for radiographic margin assessment in BCS. It is estimated²⁷ that the total number of modern digital unit installed by these three manufacturers exceeds 250 systems annually, with an installed base of several thousand units. The large installed base, as well as the rate of continued installations, indicates the clinical usefulness of intra-operative radiographic margin assessment in BCS. However, the sensitivity and specificity of intra-operative specimen radiography provided by such systems are quite low, and have been reported to be approximately 50% and 78%, respectively¹. Some of the potential equipment-related reasons for the low sensitivity and specificity of specimen radiography are: (1) Lack of convenient three-dimensional imaging, generating false negative margins; (2) False negatives generated by tissue overlap in two-dimensional projection radiography, obscuring lesion detectability; (3) Histologic false positive margins generated due to excessive specimen compression during specimen radiography. Figure 1 shows a typical portable intra-operative specimen radiography system. The excised specimen is typically placed in a specimen container, and the container is placed in the lead-shielded x-ray cabinet. A short projection cone beam of x-rays are activated for several seconds. X-rays are integrated on a high resolution solid-state detector, and the image data is processed by the system computer and displayed on a high resolution monitor within approximately 15 seconds of x-ray exposure. The image can simultaneously be sent from the Operating Room to the Radiology and Pathology Departments through a DICOM-PACS network (Digital Image Communications in Medicine – Picture Archiving and Communications Systems).



Fig. 1 – A typical intra-operative specimen radiography system (Bioptics, Inc. Tucson, AZ)

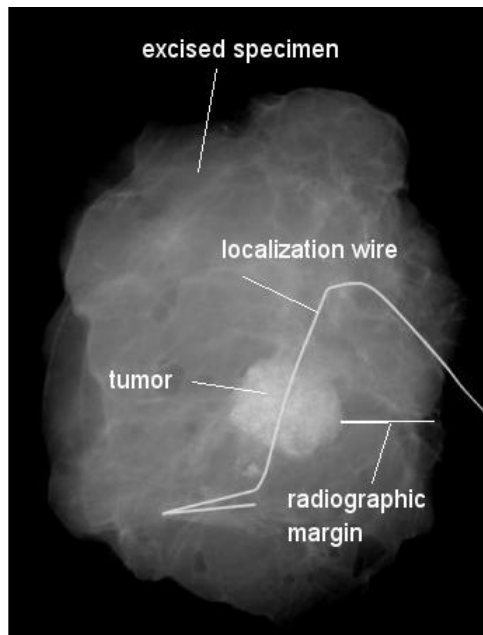


Figure 2 – A typical projection x-ray image of a surgically excised breast specimen, showing tumor and radiographic margins.

A typical projection radiograph of a surgically excised breast specimen is shown in Figure 2. The location of the tumor within the breast is identified for the surgeon by a localization wire inserted into the patient's breast pre-operatively under x-ray imaging or ultrasound guidance. The surgeon excises the tumor with a safe margin of normal tissue. The shortest distance between the edge of the tumor and the closest specimen

margin is considered to be the *radiographic* margin (as differentiated from *pathologic* margin – i.e., at the cellular level – which cannot be detected by radiology alone).

2.2 Limitations of projection radiography in margin assessment – potential for false negative margins

Figure 3 demonstrates that a single projection radiograph may not always be adequate for accurate radiographic margin assessment. While the projection image on the left shows seemingly adequate

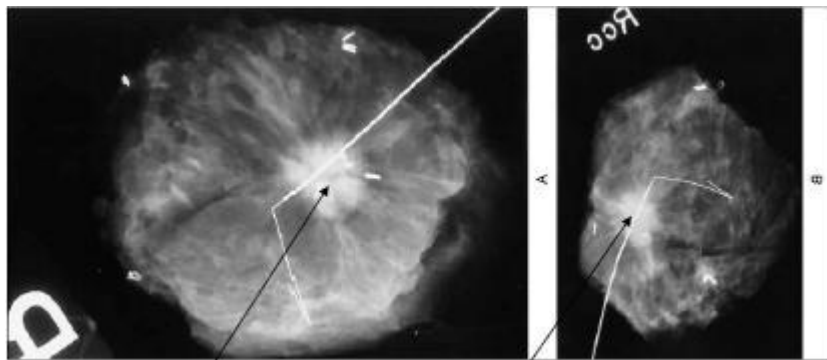


Fig. 3 – Vertical and horizontal projection specimen radiographs

margins, an additional radiograph acquired orthogonal to the original orientation shows a close margin. The orthogonal radiograph is shown on the right image of Figure 3. Ideally, in order to achieve a complete and accurate assessment of margins in all directions, three dimensional imaging such as tomosynthesis is required; however no such system exists today for BCS.

2.3 Limitations of projection radiography in margin assessment – potential for false positive margins

Breast compression is routinely employed in mammography, in order to achieve the following: (1) Reduce tissue overlap for better visualization of abnormalities; (2) Reduce overlap of normal structures whose projection image may resemble an abnormality; (3) Reduce x-ray scatter which degrades lesion detectability; (4) Reduce motion blur. Each of these benefits of compression can be applicable to specimen radiography, also. Manufacturers have therefore introduced specimen compression devices such as the TranSpec²⁸ device, shown in Figure 4.

While compression can improve lesion and radiographic margin detection, particularly in certain thick or dense excised breast tissue specimens, there is a trade-off in specimen radiography, which does not exist in mammography, namely, the displacement of tumors towards the margins of the excised specimens under compression. Tumor displacement due to compression can potentially lead to histologically false-positive

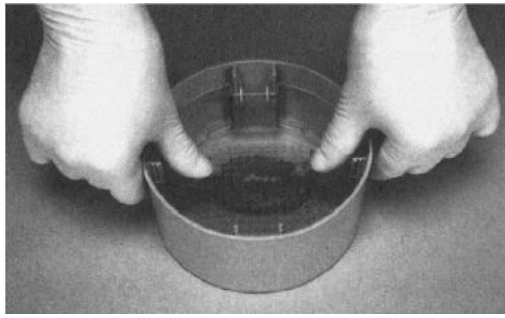


Fig. 4 – TranSpec™ BCS specimen container and compression device

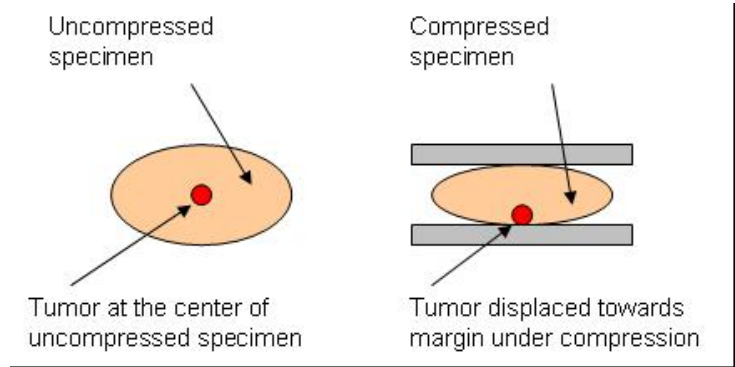


Fig. 5a – Tumor at center of uncompressed specimen

Fig. 5b – Tumor displaced towards margin of compressed specimen

margins in the direction of compression. This phenomenon is illustrated in figures 5a and 5 b. Figure 5a shows a tumor at the center of an uncompressed excised specimen. Figure 5b shows the same specimen compressed, with the tumor displaced towards the margin. Up to 63% of histologically false-positive margins have been attributed to the displacement of tumors within the specimen due to compression, leading to unnecessary surgical re-excisions²⁹. By removing overlapping tissue from the reconstructed projection images, tomosynthesis may help reduce the number of false-positive margins, and surgical re-excisions generated by excessive tissue compression.

2.4 Current research in full-breast tomosynthesis

Approximately 30% of breast cancers are missed by mammography, primarily due to the overlapped breast tissue that obscures breast cancer in conventional projection mammography³⁰. Furthermore, superimposed normal tissue can sometimes look like a tumor. It has been reported that at the Massachusetts General Hospital, the false-positive callback rate caused by superimposed normal breast tissue is approximately 25%³¹. Breast tomosynthesis is desirable over simple projection radiography by minimizing the impact of tissue overlap of projection images. There are no breast tomosynthesis systems in clinical use today, although there is active research at various academic and industry organizations in the U.S., Europe and Japan. There is also no intra-operative specimen tomosynthesis system today, even though a specimen tomosynthesis system would be relatively simpler to design for the following reasons: (1) In specimen tomosynthesis, the specimen could simply be rotated around a fixed x-ray source and detector, as opposed to rotating the heavy x-ray assembly around the patient in breast tomosynthesis; (2) In specimen tomosynthesis, the lead-shielded specimen x-ray cabinet permits acquisition of high dose (thus high signal-to-noise ratio) images. The short source-to-image distance of the specimen x-ray cabinet keeps exposure times short and the signal high. In breast tomosynthesis, each projection x-ray must be of low enough dose such that the total exposure to the patient during the full tomosynthesis sequence must not exceed the dose levels of conventional two-view projection mammography. (3) Since excised breast tissue specimens are typically much smaller than a full-breast, limited data sets will allow us to investigate more computationally intensive but better performance tomosynthesis algorithms, while keeping reconstruction times within the clinically permissible period of approximately one minute.

For reference, figures 6a and 6 b compare the geometries of full-breast and specimen tomosynthesis systems. Figure 6a shows a typical³³ full-breast tomosynthesis system geometry. In this implementation, the x-ray detector is fixed, but the x-ray source must be rotated +/-15 degrees around the patient. The x-ray source is pulsed to acquire 11 projections from equally spaced angles over a total angular range of 30 degrees. Images are reconstructed in approximately one minute with a 1 mm slice separation and 100 micron in-plane pixel size. Slices are then reviewed one at a time by mouse control or dynamically in a cine loop.

Figure 6b shows that in the specimen tomosynthesis system, x-rays are incident on the detector at a 90 degree angle, whereas in the full-breast tomosynthesis system shown in figure 6a, x-rays are incident on the detector at an oblique angle. Since oblique incidence of x-rays on a detector are known to cause resolution loss⁴⁹, the specimen tomosynthesis geometry may exhibit superior resolution, if all else is kept equal.

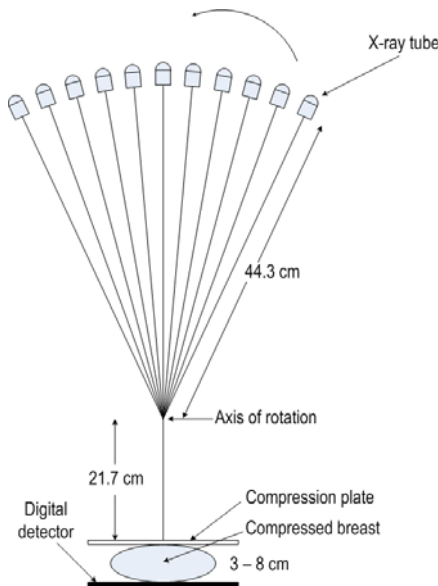


Fig. 6a – Breast tomosynthesis geometry with rotating x-ray tube assembly around the patient’s breast.

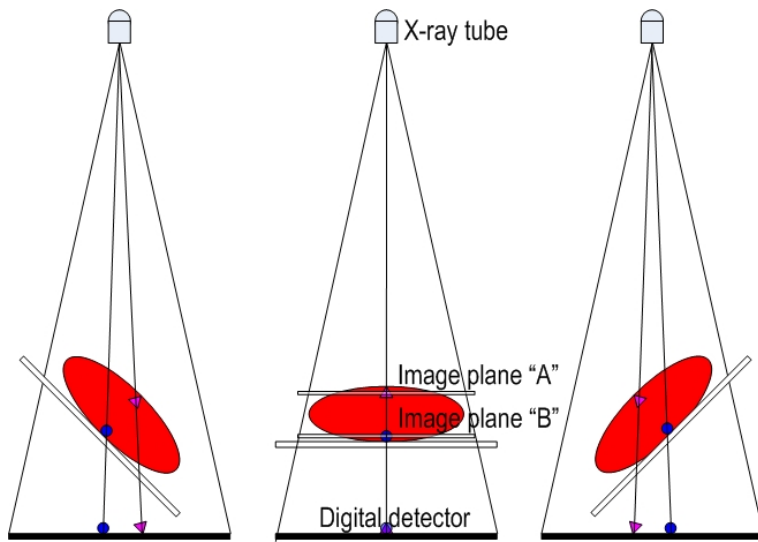


Fig. 6b – Specimen tomosynthesis geometry with fixed x-ray source and detector and motorized specimen rotation stage, demonstrating the separation of overlapping tissue necessary for tomosynthesis reconstruction.

2.5 Prior work in specimen tomosynthesis utilizing full-breast tomosynthesis devices

Figures 7a and 7b demonstrate the power of digital tomosynthesis in revealing structures that would otherwise be obscured by projection imaging. Figure 7a is a digital projection mammogram of a breast

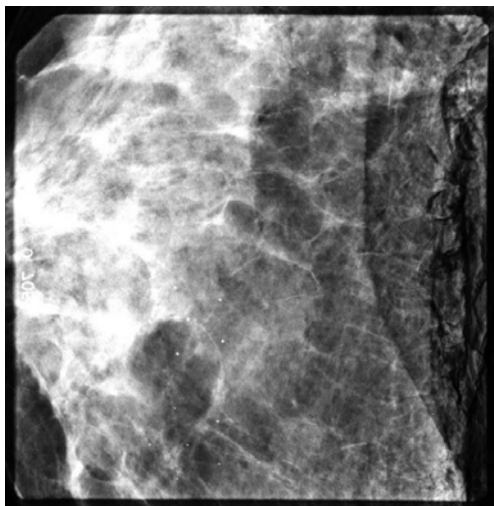


Fig. 7a – Projection radiograph of breast cadaver with phantom insert³⁰

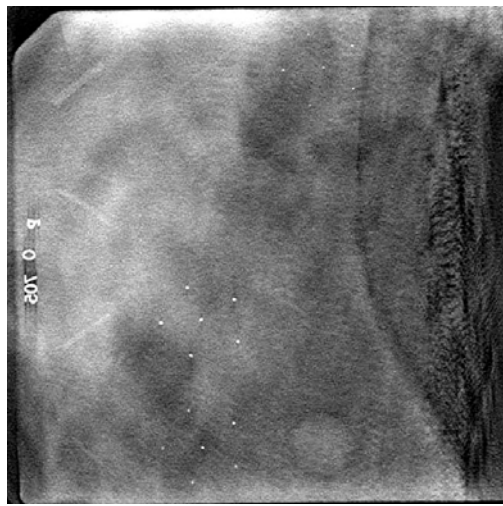


Fig. 7b – Tomosynthesis reconstruction of plane containing the phantom³⁰

cadaver with the American College of Radiology (ACR) phantom insert placed on top of the breast. Figure 7a shows that only the most conspicuous group of ACR phantom microcalcifications and the largest ACR phantom mass are detectable in the projection image, due to the presence of overlapping

tissue. Figure 7b shows that with the overlapping tissue removed from the slice containing the ACR phantom insert through tomosynthesis, most of the fibers, calcifications and masses are detectable in the tomosynthesis image. In this case, a full-field digital mammography system was modified to acquire the tomosynthesis sequence of images and the tomosynthesis images were reconstructed using a filtered back-projection method³⁰. In the proposed research, we will build and test a dedicated and portable intra-operative specimen tomosynthesis system depicted in figure 6b, and utilize this system to improve radiographic margin assessment in BCS procedures in the Operating Room.

3. Research Design and Methods

3.0 Research Design and Methods for Specific Aim 1: Specify, design and integrate hardware components of an intra-operative tomosynthesis system optimized for surgically excised breast tissue specimens in BCS.

Our design objectives for the proposed specimen tomosynthesis system are based on a literature survey of the best results that have been reported so far in full-breast tomosynthesis research:

- (1) Image reconstruction time of one minute for a maximum specimen thickness of 50 mm, 100 micron in-plane pixel size, 1 mm slice-to-slice separation, and using 11 projections³⁰.
- (2) Normalized signal-to-noise ratio for a 2mm mass of greater than 4.85, using 11 projections³¹
- (3) Normalized artifact spread function of less than 5% at 20 mm from the in-focus slice^{32,33}.

A block diagram of major hardware components needed to achieve these objectives is given in figure 8.

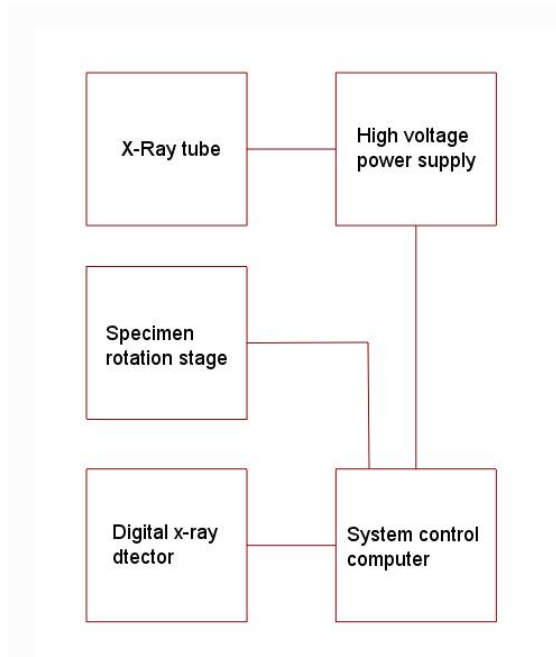


Fig. 8 – Specimen tomosynthesis system hardware components block diagram

The proposed specimen tomosynthesis system will require the seamless integration of the following five commercially available hardware components:

(1) Microfocus x-ray tube: rtw Roentgen Technik GmbH, Model MCBM 65B-50W³⁴, Berlin, Germany, or equivalent. The x-ray tube has a 50 micron micro focal spot, in order to provide high resolution images even under geometric magnification. This tungsten anode/beryllium filter tube can be operated up to 35 kV at 1 mA. This provides adequate power to ensure high signal levels at short (a few seconds) exposure times.

(2) High voltage power supply: Spellman High Voltage Electronics Corporation, Model MNX 50W x-ray power supply³⁵, Valhalla, NY, or equivalent. This 50 Watt power supply provides the required high voltage and tube current for the microfocus x-ray tube. X-ray activation can be electronically controlled via a serial interface that is a standard feature of the power supply.

(3) Specimen rotation stage: Newport Corporation, Model Agilis Series piezo driven computer-controlled rotation stage³⁶, Irvine, California, or equivalent.

The rotation stage has 360 degree continuous travel range, 5 micro-radian minimum incremental motion, and 2 degree per second maximum rotation speed under computer control.

(4) Digital x-ray detector: Rad-Icon Imaging Corporation, Model Shad-o-Box 4k³⁷, Santa Clara, California, or equivalent. This Complementary Metal-Oxide Semiconductor (CMOS) based x-ray detector has a 10 cm x 10 cm x-ray sensitive area, 10 lp/mm limiting resolution, 2.7 frames-per-second read out rate, 500 electron per analog-to-digital unit (ADU) conversion gain, and less than 1 ADU read noise.

(5) System control computer: NVIDIA Corporation, Model Quadro Plex Model II with 4 FX 5600 Graphics Processor Units (GPU)³⁸, Santa Clara, California, or equivalent. This powerful imaging and graphics processor workstation provides adequate processing power for rapid tomosynthesis reconstructions, with an 8-channel, 6 GB frame buffer.

3.1 A novel specimen container optimized for BCS specimen tomosynthesis

In order to minimize motion artifacts, the specimen must be held securely in place during the acquisition of the tomographic x-ray sequence, without applying excessive compression to the specimen. Furthermore, reconstruction artifacts can also be caused by the metallic orientation markers commonly attached to the excised specimen. To this end, we will utilize a customized specimen container, designed specifically for use in specimen tomosynthesis in BCS. Figure 9 shows a sketch of a specimen container designed specifically for use in tomosynthesis. The container is in the shape of a female breast, with a simulated nipple, a simulated sternum, a curved top surface, and a flat bottom surface. The location of the sternum identifies

whether the container to be used is for a left or a right breast. The surgeon is asked to place the excised specimen in the same orientation as it was originally in the breast. The simulated sternum identifies the medial-lateral axis of orientation of the excised specimen. The simulated nipple location defines the anterior-

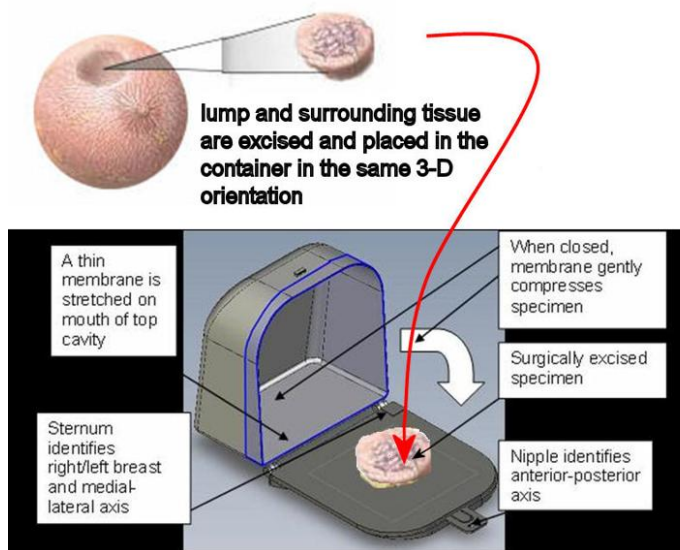


Fig. 9 – BCS container optimized for tomosynthesis

posterior axis, while the top curvature of the container identifies the superior-inferior axis. The appropriate specimen container (right or left breast, as identified by the location of the simulated sternum in the container) is opened in a clam-shell fashion, the excised specimen is placed on the bottom piece, in the same orientation as the specimen was excised from the breast and the container is closed. The thin and flexible membrane stretched across the top cavity of the container conforms to the shape of the specimen when the container is closed, thus holding the specimen firmly in place while it is rotated during the acquisition of the tomosynthesis image sequence, without excessive compression. Spatial orientation markers built into the container obviate the need to use metallic orientation clips which may cause reconstruction artifacts.

The specimen container is designed to display the orientation of the specimen in the breast, prior to surgical excision. To this end, Figure 10a and 10b compare a standard cranio-caudal (CC) view of the breast to the

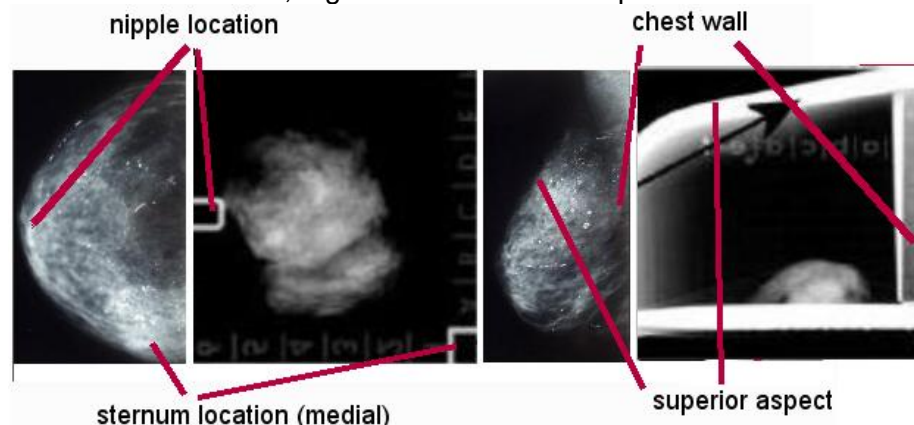


Fig. 10a – “CC” view of a right breast

Fig. 10b – “CC” view of specimen from a right breast in the container

Fig. 10c – “ML” view of a right breast

Fig. 10d – “ML” view of specimen from a right breast in container

“CC” view of the container respectively. Similarly, figures 10c and 10d compare a standard medio-lateraloblique (MLO) view of the breast to the “MLO” view of the specimen container, respectively. The container conveys three dimensional orientation information by utilizing a simulated sternum, nipple, chest wall and breast curvature on the superior aspect of the breast, which can be observed in the “CC” and “MLO” radiographs of the container given in figures 10b and 10d.

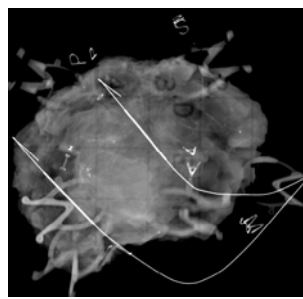


Fig. 10e – Use of orientation clips, which can create tomo artifacts

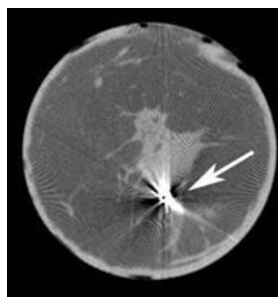


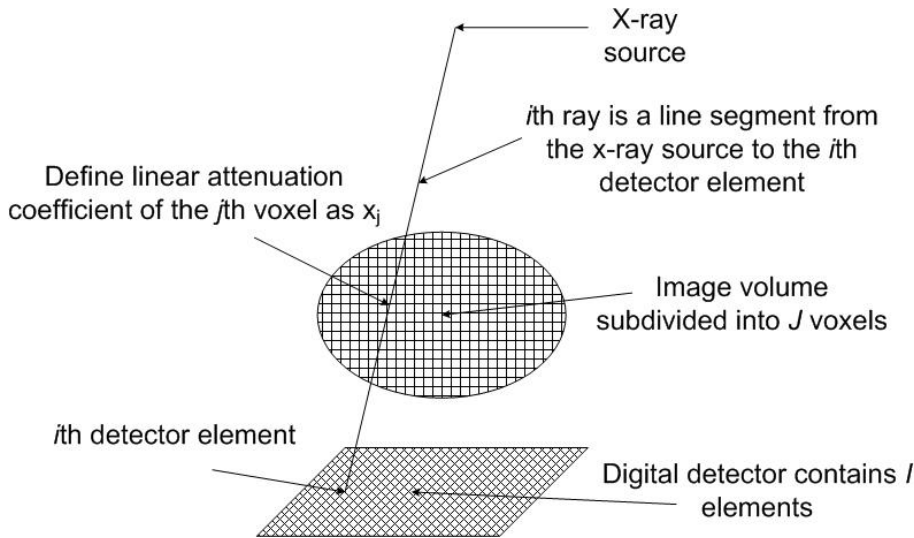
Fig. 10f – Example of a tomo artifact created by a clip

The simulated sternum, nipple, chest wall and breast curvature built into the specimen container define specimen orientation in three dimensions. Without the specimen container, orientation information is provided through the use of metallic markers, labeled “cranial,” “caudal,” “medial,” “lateral,” etc. A specimen with such metallic markers is shown in figure 10e. In addition to potentially obscuring the specimen, these metallic markers often generate streak artifacts in tomosynthesis reconstruction, as shown in figure 10f. Elimination of the metal clips through the use of the proposed specimen container would improve tomosynthesis reconstruction by eliminating this source of artifacts.

4.0 Research Design and Methods for Specific Aim 2: Specify, design and implement software algorithms optimized for rapid and accurate intra-operative tomosynthesis of surgically excised breast tissue specimens in BCS.

While the hardware specified above will yield low noise projection images acquired in within a few seconds, successful completion of specific aim 2 will require the development of rapid and accurate reconstruction software algorithms which meet the design objectives specified in Section 3.0.

The linear system model to be used in the development of the specimen tomosynthesis reconstruction software algorithm will be built upon the methods described by Zhang and colleagues³⁹, as shown in figure 11.



As shown in Figure 11, in order to develop a linear systems model for specimen tomosynthesis, the subject volume is first subdivided into J voxels. The linear attenuation of the j th voxel is defined as x_j . The digital detector is subdivided into I pixels. The x-ray beam from the point x-ray source (a good approximation of a micro-focus x-ray source in our implementation) to the i th pixel is defined as the i th ray. The path length of the i th ray going through the j th voxel in the n th

Fig. 11 – Linear systems model for specimen tomosynthesis³⁹.

specimen orientation is denoted by $a_{ij,n}$, resulting in a matrix-vector form of the projection model as $\mathbf{A}_n \mathbf{x} = \mathbf{y}_n$, where \mathbf{A}_n is the projection matrix for the n th projection view with $a_{ij,n}$ as its (i,j) th element and \mathbf{y}_n is the corresponding vector of the projection data. The i th projection value, $y_{i,n}$, is proportional to the log transform of the ratio of the incident intensity $I_{o,n}$ and the transmitted x-ray intensity $I_{i,n}$ of the i th ray, as $y_{i,n} = k \ln(I_{o,n}/I_{i,n})$ where k is a system independent proportionality constant.

Most commonly used breast tomosynthesis algorithms have been described in detail in the literature, including various implementations and their relative performance in terms of signal-to-noise ratio, signal-to-background ratio, artifact spread function, modulation transfer function, reconstruction time, and other relevant parameters. These algorithms include: (a) shift-and-add technique^{40, 41, 42, 43}, which is the simplest and most intuitive technique that is similar to the unfiltered backprojection method. It is computationally fast and delivers a high signal difference to noise ratio, but can also generate streak artifacts which need to be suppressed. (b) Filtered backprojection technique^{44, 40, 45, 43, 39}, which is a technique which delivers high contrast-to-noise ratio and high edge sharpness for microcalcifications, but relatively poor image quality for masses. Filtered backprojection techniques can also create blurring artifacts, which must be suppressed. (c) Algebraic reconstruction technique^{40, 45, 42}, which is a computationally extensive iterative technique, which provides high signal-to-background ratio, good artifact suppression, and good contrast enhancement for both masses and microcalcifications. (d) Maximum likelihood expectation maximization technique^{45, 42, 39}, which is another iterative technique that provides high quality images with good contrast enhancement, but is computationally the most complex algorithm.

With adequate processing hardware, image reconstruction times of one minute have been reported for full-breast tomosynthesis for a 50 mm breast at 0.1 mm in-plane pixel size, and 1 mm slice-to-slice separation³⁰. Since excised specimens are typically significantly smaller than a full breast, image data sets will be correspondingly lower, enabling shorter processing times, and/or the use of more computationally intensive and higher performance tomosynthesis reconstruction algorithms.

4.1 Specimen tomosynthesis simulations and reconstruction

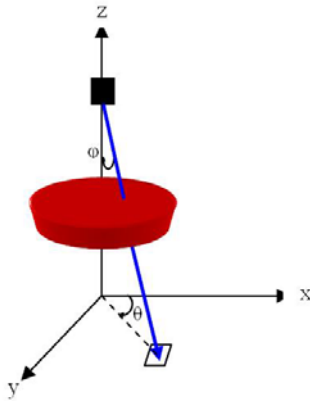


Fig. 12 – Tomosynthesis simulation geometry

We will utilize computer simulations to assess the efficacy of our selected tomosynthesis reconstruction algorithms. Tomosynthesis can be simulated by integrating attenuation coefficients $\mu(x, y, z)$ along the path of the rays originating from the x-ray source to a pixel in the detector. For the purposes of simulation, we will assume the x-ray source to be a point source, which is a good approximation for the 50 micron x-ray tube we plan to use in our studies. Let (x_0, y_0, z_0) be the location of the x-ray source and (x_p, y_p, z_p) be the location of the p th pixel on the detector. While x_0 and y_0 could be set equal to zero by assuming that the x-ray source is co-centric with the x-ray detector, we have selected to keep the notation generalized for simulation purposes. Each ray can be indexed by two angles (φ, θ) , where α is the angle between the projection of the ray on the xy plane and the x -coordinate, as shown in figure 12.

Considering the ray that connects the x-ray source with the p^{th} detector pixel, let (φ_p, θ_p) be the angles that are used to index this ray. φ_p and θ_p can be computed using expression (1a) and (1b).

$$\varphi_p = \tan^{-1} \left(\frac{|z_p - z_0|}{\sqrt{(x_p - x_0)^2 + (y_p - y_0)^2}} \right) \quad (1a) \quad \text{and} \quad \theta_p = \tan^{-1} \left(\frac{|y_p - y_0|}{|x_p - x_0|} \right) \quad (1b)$$

The angles (φ_p, θ_p) can be corrected according to their quadrants inferred from the coordinates of the x-ray source and the detector, as shown in expressions (2a) and (2b):

$$\varphi_p^{\text{corrected}} = \begin{cases} \varphi_p & z_p \geq z_0 \\ \pi - \varphi_p & z_p \leq z_0 \end{cases} \quad (2a) \quad \text{and} \quad \theta_p^{\text{corrected}} = \begin{cases} \theta_p & x_p \geq x_0, y_p \geq y_0 \\ \pi - \theta_p & x_p < x_0, y_p \geq y_0 \\ -\theta_p & x_p \geq x_0, y_p < y_0 \\ -\pi + \theta_p & x_p < x_0, y_p < y_0 \end{cases} \quad (2b)$$

Once the angles of a ray from the x-ray source to the p^{th} detector are corrected, the x-ray intensity on the detector, I_p can be computed as shown in expression (3):

$$I_p = I_0 e^{-\int \mu(\tau \sin(\varphi_p) \cos(\theta_p), \tau \sin(\varphi_p) \sin(\theta_p), \tau \cos(\varphi_p)) d\tau} \quad (3)$$

where τ is the distance traveled by the ray originating from the x-ray source, and μ is the attenuation coefficient.

Equation (3) can be expressed in discrete form, as shown in expressions (4) and (5):

$$\mu_p^{\text{total}} = \Delta \tau \sum_{k=0} \mu(x_0 + k\Delta \tau \sin(\varphi_p) \cos(\theta_p), y_0 + k\Delta \tau \sin(\varphi_p) \sin(\theta_p), z_0 - k\Delta \tau \cos(\varphi_p)) \quad (4)$$

$I_p = I_0 e^{-\mu_p^{\text{total}}}$ (5) where $\Delta \tau$ is a fixed incremental distance (0.1 mm in the simulations) over which the attenuation coefficient μ is assumed to be constant, and k is the summation index.

To perform the simulations, we created a synthetic phantom and forward projected it using the formulation described above. Figure 13a shows the computer-simulated phantom. The phantom has three spheres with three different attenuation coefficients.

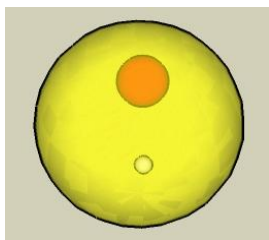


Fig. 13a – Tomosynthesis computer-simulation phantom with overlapping objects.

A big background sphere of 50 mm in diameter simulates the excised specimen. Inside this sphere, at coordinates (0,0,0) we embedded a smaller sphere 10 mm in diameter, simulating a large tumor. Another smaller sphere, 3 mm in diameter was centered at (0, 20 mm, -10 mm), simulating a smaller tumor. The smaller sphere located at $z=-10$ mm was completely occluded by the larger sphere at $z=10$ mm in a projection image. The center of rotation was assumed to be the origin (0,0,0) of the three dimensional coordinate system. Projections were computed from 10 different angles ranging from -45 degrees to +45 degrees in steps of 10 degrees. Some of these projections are shown in figure 13b. For these projections, the x-ray source was assumed to be located at (0,0, 180mm), and the detector was located on the xy plane at $z = -20$ mm. Each voxel was 1 mm x 1 mm x 1 mm for the purposes of the simulation.

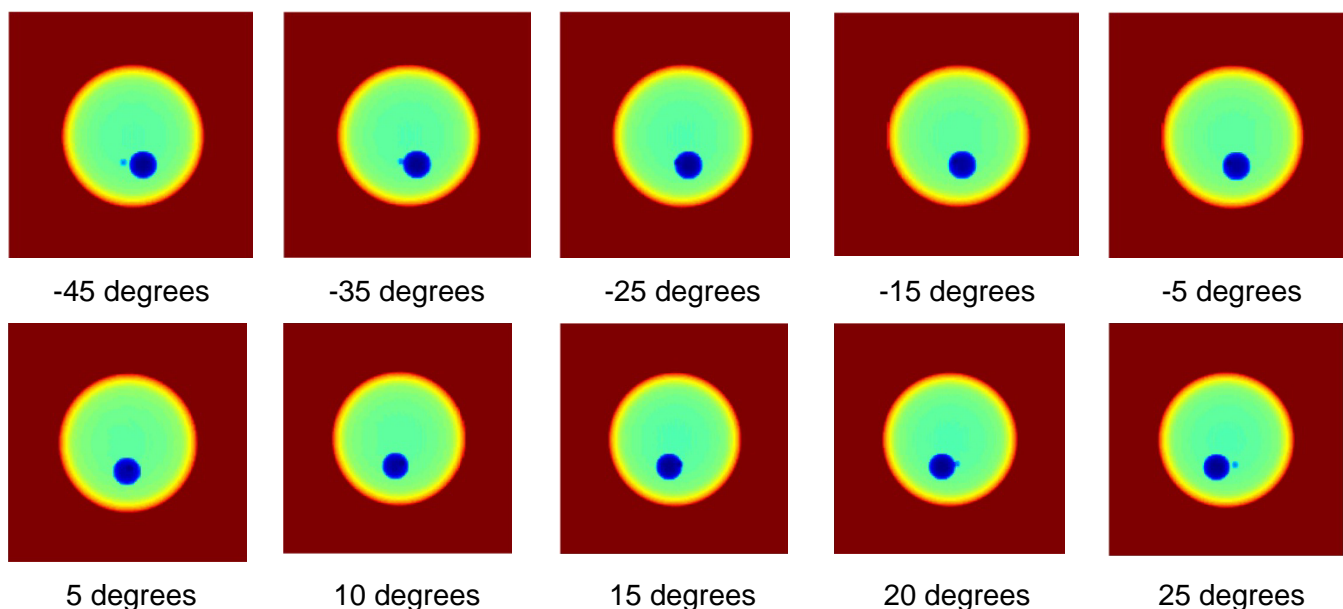


Fig. 13b – Selected simulated projection images of two tumors in a simulated excised specimen, where the smaller tumor is completely occluded by the larger tumor in most projection images.

The projections were then reconstructed using a multiple-projection algorithm (MPA) as described by Kolitski and colleagues^{46, 47}. Reconstructions for $z = 10$ mm and $z = -10$ mm are shown in figure 14a through 14d. The out of focus plane blur can be seen in these reconstructions. Using the out-of-focus blur removal algorithm described by Kolitski^{46, 47}, we were able to remove some of the blur from these reconstructions. This example is given here to illustrate our tomosynthesis simulation capabilities. During the course of the proposed research, we will utilize and simulate other more sophisticated algorithms to suppress out-of-focus plane blur more effectively.

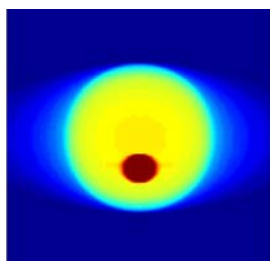


Fig. 14a – Reconstructed plane of large tumor; with deblurring

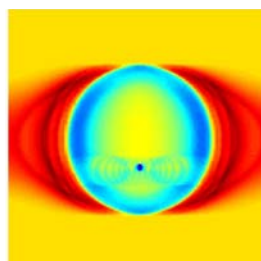


Fig. 14b – reconstructed plane of small tumor; with deblurring

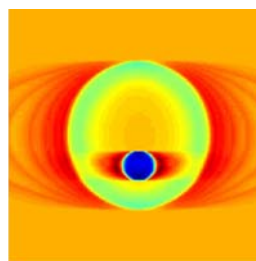


Fig. 14c – Reconstructed plane of large tumor; without deblurring

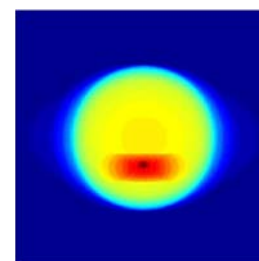


Fig. 14d – Reconstructed plane of small tumor; without deblurring

Figure 15a and 15b show a typical simulation geometry to quantify the efficacy of our selected tomosynthesis reconstruction algorithms in removing needle artifacts from reconstructed slices. As indicated previously, most surgically excised breast tissue specimens will contain a localization wire inside them, thus it is important for the tomosynthesis reconstruction software to effectively remove artifacts arising from the needle from the reconstructed images. Figure 15b shows a computer simulation of a reconstructed slice through a simulated tumor. Note that even though this slice is 10 mm away from the actual location of the needle, its artifacts are clearly visible in the slice of interest, obscuring the detectability of the tumor. We will investigate several reconstruction algorithms^{31, 32} and image acquisition geometries such as dual axes rotation, to minimize such metal artifacts.

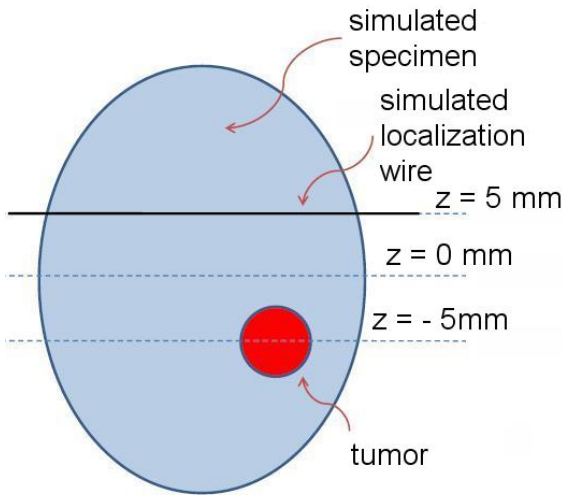


Fig. 15a – Simulated specimen with tumor and localization needle

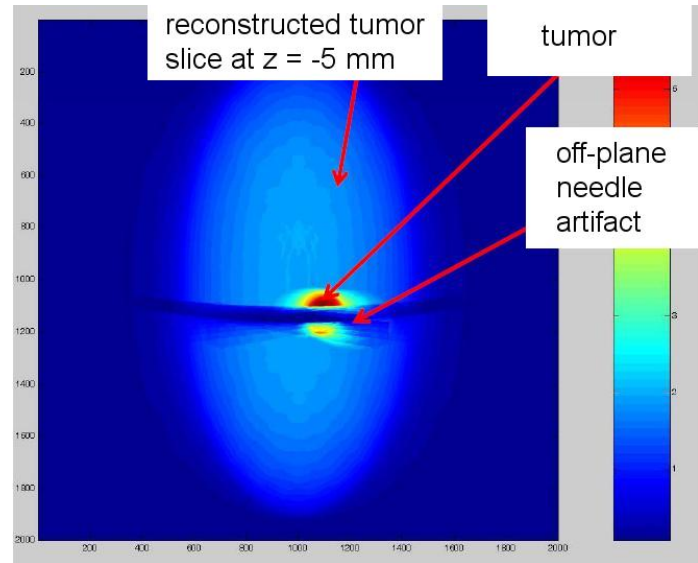


Fig. 15b – Off-plane needle artifacts obscuring tumor without artifact suppression

With further processing (interpolating out the needle from the projection images, as an example), it is possible to suppress needle artifacts from the reconstructed images, as shown in figures 16a and 16b. We will investigate other artifact suppression algorithms described in the literature³⁹⁻⁴⁷ during the proposed research.

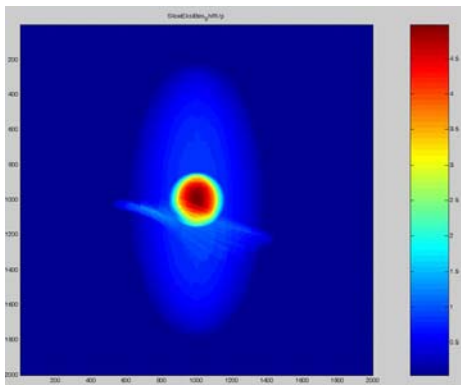


Fig. 16a – Off-plane needle artifact with no processing

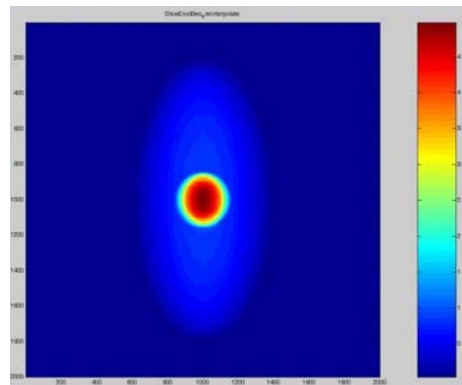


Fig. 16b – Off-plane needle artifact suppression

Figure 16a shows the presence of an off-plane needle artifact in the plane of the tumor within the specimen. Figure 16b shows the same plane with the needle artifact suppressed by interpolating out the needle with neighboring pixel intensity values from the original projection images. Interpolation of

the needle may be clinically acceptable, since there is no relevant image data under the needle in the original radiograph, where x-rays are completely attenuated by the metallic localization needle. Other strategies to remove tomosynthesis artifacts generated by high attenuation features such as metal clips, localization wires, and even high density calcifications have been reported in the literature. For example, Wu and colleagues have described a “voting” strategy algorithm³¹, which has been shown to effectively suppress such artifacts from tomosynthesis reconstructions. In the proposed Phase I study, we will investigate the efficacy of the “voting” strategy and other algorithms to suppress artifacts in both computer-simulated specimens, as well as physical specimens constructed from various materials simulating human breast tissue, such as ground turkey breast and unleavened bread dough.

5.0 Research Design and Methods for Specific Aim 3a: Integrate selected hardware and software components optimized for intra-operative tomosynthesis of surgically excised breast tissue specimens in BCS.

Successful completion of Specific Aim 3 will result in a fully integrated system, with all software and hardware components working seamlessly together, such that when the user places a specimen container within the x-ray cabinet and initiates system operation with one mouse click, the desired number of consecutive projection x-ray images of the specimen are automatically acquired as the specimen is rotated to desired angles; acquired images are corrected and reconstructed; and the tomosynthesis slices are displayed plane-by-plane on the high resolution system monitor – all within less than three minutes.

Figure 17 shows a system integration block diagram, showing each of the software and hardware components of the system and their respective interfaces.

In order to focus our efforts primarily on the novel research and development aspects of the proposed study, we will utilize standard, commercially available third party imaging software for x-ray image acquisition, display, analysis, archival and communications, rather than attempting to develop it ourselves. This approach will enable us to concentrate on developing novel algorithms for specimen tomosynthesis, and for system integration. There are many third party medical imaging software packages available; Cedara Corporation of Ontario, Canada offers its Cedara I-ReadMammo™ software development package, which features a complete set of tools to acquire, calibrate, display x-ray images (including zoom, pan, invert, annotate, window/level, etc.), and to transfer, print and archive the images acquired in standard Digital Imaging in Communications (DICOM) format over a standard Picture Archiving and Communications (PACS) network.

While we will utilize commercially available software tools for image acquisition, display, analysis, communications, and archival, as part of the proposed research we will develop our own interface between the specimen tomosynthesis hardware, tomosynthesis software, and the third party standard imaging software.

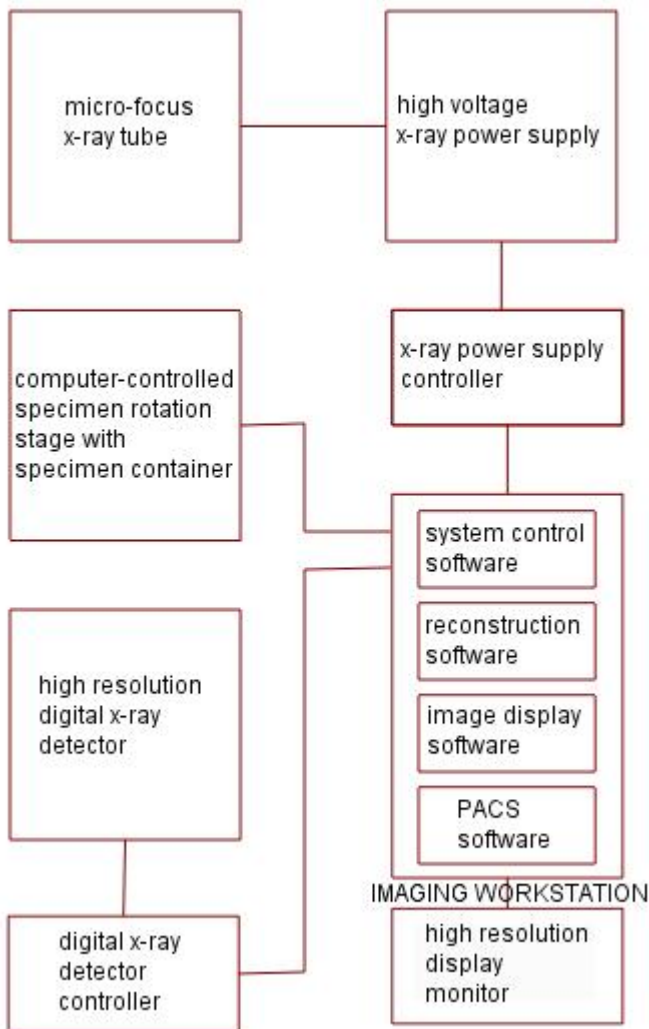
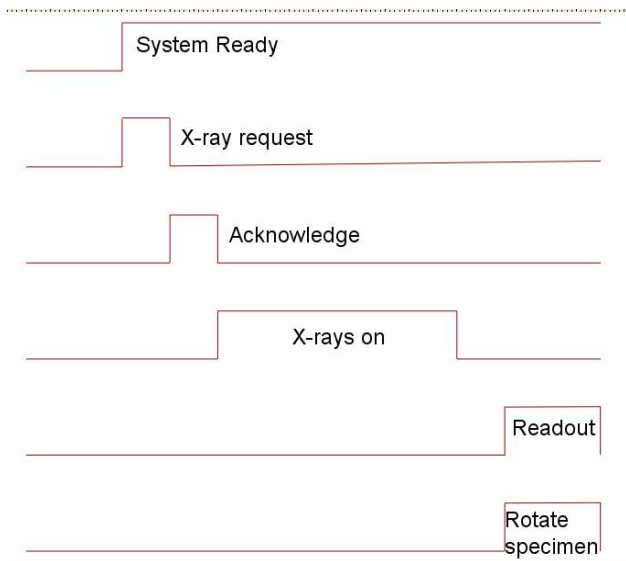


Fig. 17 – System Integration Block Diagram

A timing diagram of the electronic synchronization signals, which will form the basis of the system integration control software and hardware, is given in figure 18. Acquisition of a sequence of projection x-ray images at prescribed rotation angles will require careful synchronization of the x-ray source, specimen rotation stage, and the digital x-ray detector.



Since each major component of the system is available with sophisticated electronic input/output controls, our task will be to design control software which will instruct the motorized rotation stage to rotate the specimen to any desired angle with respect to the fixed x-ray source and detector; pulse the x-ray source for a desired period, during which time the digital x-ray detector will be placed in signal integration mode. At the conclusion of the x-ray pulse, the digital x-ray detector will be read out on a pixel-by-pixel basis, while the specimen is rotated to the next desired angle. The acquired projection images will be gain and offset corrected, and reconstructed. The reconstructed slices will be displayed plane-by-plane on the imaging workstation monitor.

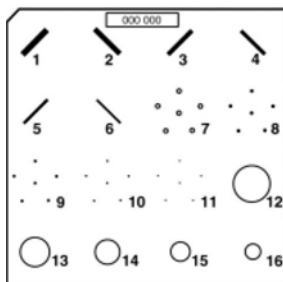
Fig. 18 – System synchronization timing diagram

Since tomosynthesis reconstruction may take up to one minute, the first projection x-ray image of the specimen acquired at 0 degrees will be immediately displayed on the workstation monitor for the surgeon’s initial review. If the surgeon is satisfied with this projection image, he/she will click on a button labeled “proceed with tomosynthesis image sequence acquisition.” If the surgeon wishes to acquire more single projection images of the specimen at any other desired angle, he/she will be able to do so before initiating corresponding image. the tomosynthesis image acquisition sequence. Once the sequence of projection x-ray images are acquired into memory and reconstruction is completed, the user will be able to display each slice in a “cine” type automatic loop, or manually display each slice on at a time. The depth of each slice from the surface of the specimen will be displayed on the monitor along with the corresponding displayed specimen plane.

6.0 Research Design and Methods for Specific Aim 3b: Quantify the integrated system’s efficacy in a pre-clinical setting, utilizing simulated excised breast tissue samples and standard breast x-ray imaging phantoms.

In order to demonstrate the basic technical feasibility of the specimen tomosynthesis system in Phase I of this research, we will image simulated specimens as opposed to actual patient specimens. We will conduct a formal clinical trial with patient specimens in Phase II of the research, after ensuring that the system meets the system-level design objectives identified in section 3.

For pre-clinical evaluation of the specimen tomosynthesis system and testing the efficacy of various tomosynthesis software algorithms, we will use the wax insert of the standard American College of Radiology (ACR) mammography accreditation phantom⁴⁸, the contents of which are shown in figure 19a and described in figure 19b.



- | | |
|------------------------|--------------------|
| 1. 1.56 mm nylon fiber | 9. 0.32 mm specks |
| 2. 1.12 mm nylon fiber | 10. 0.24 mm specks |
| 3. 0.89 mm nylon fiber | 11. 0.16 mm specks |
| 4. 0.75 mm nylon fiber | 12. 2.00 mm specks |
| 5. 0.54 mm nylon fiber | 13. 1.00 mm mass |
| 6. 0.40 mm nylon fiber | 14. 0.75 mm mass |
| 7. 0.54 mm specks | 15. 0.50 mm mass |
| 8. 0.40 mm specks | 16. 0.25 mm mass |

The ACR mammography accreditation phantom consists of two components. A 55 mm thick acrylic base, simulating the attenuation and scatter characteristics of a typical breast, and a wax insert with embedded objects which simulate microcalcifications, spiculations, and masses. Since the acrylic base is a

Fig. 19a – ACR phantom

Fig. 19b – Description of the ACR mammography phantom contents

uniform material, it will not accurately reflect the overlapping tissue properties of a real breast, or a real breast specimen. We will therefore use only the wax insert of the ACR phantom, which contains the objects of

interest to us. We will replace the 55 mm thick acrylic block of the ACR phantom with various thicknesses of combinations of ground pork fat and turkey breast in order to simulate overlapping breast tissue of various densities more realistically. The resulting phantom set-up is shown in figure 20a. Figure 20b shows a radiograph of the ACR phantom with no overlapping tissue, where most of the phantom objects are easily detectable. Figure 20c shows the same phantom placed inside 5 cm of ground turkey breast, simulating the overlapping tissue of excised breast specimens. Only the largest of the phantom objects are detectable in figure 20c, due to the obscuring of the objects by overlapping tissue. With tomosynthesis, we will be able to reconstruct and display the plane containing the ACR phantom. Since the contribution of overlapping tissue projections to the selected plane will be minimized, tomosynthesis is expected to improve the detectability of the phantom objects significantly.

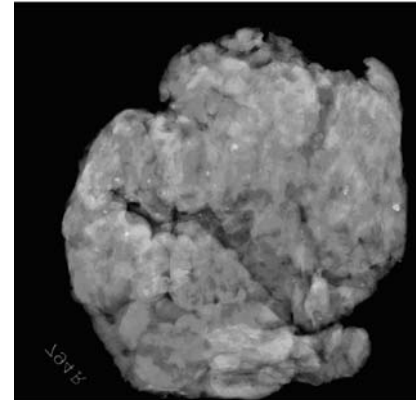
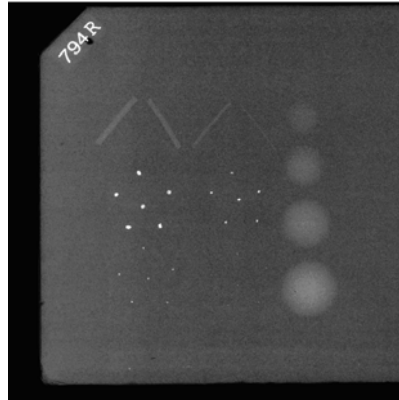
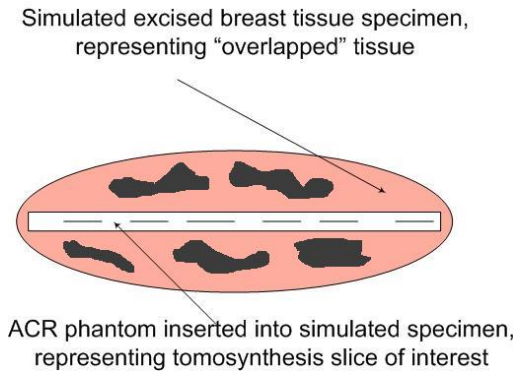


Fig. 20a – Specimen tomosynthesis evaluation phantom, with ACR phantom insert inside simulated overlapping breast tissue.

Fig. 20b – Radiograph of ACR phantom wax insert alone, with no overlapping tissue

Fig. 20c – Radiograph of ACR phantom wax insert placed inside 5 cm of overlapping turkey breast tissue

In addition to the ACR phantom, we will also insert a thin metal wire (~ 1 to 2 mm diameter) in the simulated specimen. The purpose of the wire is to simulate the localization wire commonly found in most excised breast tissue specimens. The localization wire generates off-plane artifacts in the tomosynthesis images, which must be suppressed using appropriate software algorithms.

We will acquire a series of angulated projection x-ray images of the phantom consisting of the ACR wax insert embedded in ground turkey breast tissue, and reconstruct the slice(s) containing the wax insert. We will then be able to quantitatively compare the detectability of the phantom objects with tomosynthesis, as compared to simple projection radiography.

Parameters that will be measured will be the signal-to-noise ratio (SNR), signal-to-background ratio (SBR), and the artifact spread function (ASF). Methods for measurements of these parameters have been described in detail by Rakowski and colleagues³³, and we will follow their methodologies in making these measurements. Parameters measured in the reconstructed images, as well as the total dose, will be normalized to their respective values in the original projection x-ray image. Objects embedded in the ACR phantom provide a very convenient means of experimentally measuring performance characteristics and have therefore been used in many studies. We will vary the thickness of overlapping tissue from 10 mm to 50 mm in 5 mm increments in order to determine the impact of object thickness on the efficacy of selected tomosynthesis algorithms. We will plot SNR, SBR and ASF as functions of tissue thickness, number of projection images, and type of tomosynthesis reconstruction algorithm tested during Phase I. Since we will not be utilizing actual patient specimens in Phase I studies, we will have the luxury of testing the performance of the system and reconstruction algorithms with hundreds of simulated specimens of various sizes and densities. At the conclusion of the Phase I study, we will select the algorithm which optimizes SNR, SBR and ASF in our selected hardware configuration and at the same time satisfies our clinical goal of displaying tomosynthesis images within two to three minutes of excision.